Design and characterization of dielectric filled TM_{110} microwave cavities for ultrafast electron microscopy

Review of Scientific Instruments

Design and characterization of dielectric filled TM_{110} microwave cavities for ultrafast electron microscopy

Cite as: Rev. Sci. Instrum. **90**, 083703 (2019); https://doi.org/10.1063/1.5080003
Submitted: 05 November 2018 . Accepted: 04 August 2019 . Published Online: 20 August 2019

W. Verhoeven, J. F. M. van Rens, A. H. Kemper, E. H. Rietman, H. A. van Doorn, I. Koole, E. R. Kieft, P. H. A. Mutsaers, and O. J. Luiten

AIP Publishing

Review of Scientific Instruments ARTICLE scitation.org/journal/rsi

Design and characterization of dielectric filled TM_{110} microwave cavities for ultrafast electron microscopy

Cite as: Rev. Sci. Instrum. 90, 083703 (2019); doi: 10.1063/1.5080003
Submitted: 5 November 2018 • Accepted: 4 August 2019 •
Published Online: 20 August 2019

W. Verhoeven,[1] J. F. M. van Rens,[1] A. H. Kemper,[1] E. H. Rietman,[1] H. A. van Doorn,[1] I. Koole,[1] E. R. Kieft,[2] P. H. A. Mutsaers,[1] and O. J. Luiten[1,a)]

AFFILIATIONS

[1] Department of Applied Physics, Coherence and Quantum Technology Group, Eindhoven University of Technology, P.O. Box 513, 5600 MB Eindhoven, The Netherlands
[2] Thermo Fisher Scientific, Achtseweg Noord 5, 5651 GG Eindhoven, The Netherlands

[a)] **Electronic mail:** o.j.luiten@tue.nl

ABSTRACT

Microwave cavities oscillating in the TM_{110} mode can be used as dynamic electron-optical elements inside an electron microscope. By filling the cavity with a dielectric material, it becomes more compact and power efficient, facilitating the implementation in an electron microscope. However, the incorporation of the dielectric material makes the manufacturing process more difficult. Presented here are the steps taken to characterize the dielectric material and to reproducibly fabricate dielectric filled cavities. Also presented are two versions with improved capabilities. The first, called a dual-mode cavity, is designed to support two modes simultaneously. The second has been optimized for low power consumption. With this optimized cavity, a magnetic field strength of 2.84 ± 0.07 mT was generated at an input power of 14.2 ± 0.2 W. Due to the low input powers and small dimensions, these dielectric cavities are ideal as electron-optical elements for electron microscopy setups.

I. INTRODUCTION

A. Ultrafast electron microscopy

Since the formulation of Scherzer's theorem in 1936,[1,2] which states that rotationally symmetric electro- and magnetostatic lenses will always have positive spherical aberrations, researchers have proposed different methods of incorporating time-varying fields inside an electron microscope to correct for these aberrations. However, due to the difficulty in generating rapidly varying fields at that time, the actual current that could be transmitted was too low in these schemes to make them viable. In the 1970s, with the availability of microwave technology, interest in pulsed electron beams started to grow again. Oldfield[3] and Ura and Morimura[4] both independently managed to implement a two step method to create and then bunch electron pulses at gigahertz repetition rates, achieving subpicosecond pulse lengths.[5]

Nowadays, interest in microwave cavities is on the rise again with the introduction of time-resolved electron experiments. Inside an ultrafast electron microscope (UEM), subpicosecond resolution can be added to powerful techniques such as direct electron imaging,[6,7] diffraction,[8,9] energy spectroscopy,[10,11] and Lorentz microscopy.[12] In these setups, microwave cavities can be used to improve the temporal resolution,[13] as a streak camera,[14,15] or for time-of-flight spectroscopy.[16,17]

The generation of electron pulses inside an UEM is typically done using photoemission, with which pulse lengths down to 200 fs can be achieved.[18] However, several blanking methods are emerging as an alternative, in which an electron beam is periodically deflected over a small slit or aperture.[19–21] These methods have the advantage that no alterations have to be made to the electron source. Recently, it has been shown both theoretically[19,22] and experimentally[17] that electron pulses can be created by deflecting a continuous beam over a slit with a TM_{110} cavity while maintaining the emittance and energy spread of the continuous electron source. This is achieved by using a conjugate blanking scheme, resulting in high quality ultrashort pulses. Using state-of-the-art synchronization

systems, the microwave signal can be synchronized to a laser pulse,[23–25] allowing for pump-probe experiments to be performed with a good spatial resolution and a temporal resolution in the range of 100 fs.

Figure 1(a) schematically shows the principle of chopping with a microwave cavity. Inside the cavity, electromagnetic standing waves can be resonantly generated. When exciting the TM_{110} mode, this standing wave has a transverse oscillating magnetic field on the axis of the cavity and no electric field. When electrons move through this field, the Lorentz force will periodically deflect the electron beam. By placing a slit at a distance, ultrashort pulses can be created from the continuous beam.

Microwave cavities operate at frequencies in the gigahertz regime, resulting in electron pulses at a high repetition rate and therefore a high duty cycle. This can be utilized by also pumping a sample with microwaves, providing a large average current.[20] Furthermore, it has been shown that pulsing of an electron beam can reduce damage mechanisms in beam sensitive materials, both for pulses chopped with a cavity[26] or pulses created through photoemission.[27] Here, the high frequency achievable with a microwave cavity might allow for the investigation of beam sensitive materials with relatively large currents.

Although the high repetition rate is an advantage in some situations, typical UEM experiments are performed at few tens of megahertz[28] down to few tens of kilohertz[29] repetition rates, to allow for the investigation of processes with relaxation times of nanoseconds to microseconds. Since a cavity operating at these frequencies would have impractically large dimensions, it has been proposed to deflect the beam in two directions at different harmonics of the desired repetition rate, allowing for electron pulses to be created at the difference frequency.[19] This principle is shown in Fig. 1(b), which schematically depicts an electron beam being deflected by two harmonics of a fundamental frequency f_0, resulting in a deflection following a Lissajous pattern which is traced by the electron beam at this fundamental frequency. By placing an aperture at the center, shown here in red, pulses can then be created at the lower frequency f_0. By using a cavity that can support both frequencies, these Lissajous patterns can be created with a single cavity. This principle has also been experimentally demonstrated inside an UEM to reduce the repetition rate to 75 MHz using the 40th and 41st harmonic of a laser oscillator.[30]

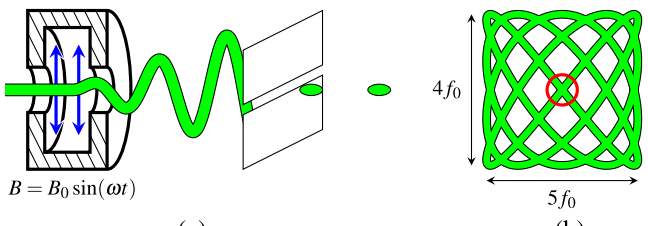

FIG. 1. (a) Principle of beam chopping using a cavity. The oscillating magnetic field periodically deflects the electron beam over a slit, resulting in ultrashort electron pulses. (b) By deflecting the beam in perpendicular directions with two different frequencies both locked to a frequency f_0, the electron beam passes a pinhole (shown in red) at the difference frequency.

B. Dielectric cavities

Application of microwave cavities to manipulate electron beams at energies of 30–300 keV typically requires input powers in the range of 10^2–10^3 W, for which expensive amplifiers are needed. Furthermore, this requires cooling systems with a high capacity to dissipate all the power, which can cause unwanted vibrations. Therefore, streak cavities can be filled with a dielectric material, reducing both the size and the power consumption of the cavity.[31] This is shown in Table I, where the size and power consumption of vacuum and dielectric cavities are compared. Shown here are both the theoretical values of a cylindrical cavity, also called a pillbox cavity, and measurements performed on cavities that are optimized for power consumption. For the vacuum cavity, optimization is done by deviating from the pillbox geometry. This design is reported in Ref. 32. The dielectric cavity is optimized by optimizing the dielectric filling ratio, and is reported here. Due to the incorporation of the dielectric, generation of 100 fs pulses, which requires field strengths of ~3 mT, can be achieved with an input power of only ~16 W.

Although the design and implementation of a dielectric filled cavity was reported before in Ref. 31 as a proof-of-principle, this cavity proved to be difficult to reproduce. This makes it impossible to synchronize the microwave fields to a laser, since synchronization systems make use of components with a very narrow bandwidth.[23–25] Synchronization to a laser therefore requires a well-defined resonant frequency of the cavity. The system reported, e.g., in Ref. 23 uses components with a bandwidth of 2 MHz. Driving a cavity with this system therefore requires a precise control over the resonant frequency.

Although this precision can be easily achieved for a vacuum cavity using accurate machining, it becomes much more difficult when incorporating a dielectric material. The main difficulty in fabricating a dielectric cavity lies in the fact that the entire surface of the metal housing enclosing the dielectric has to be electrically connected, but it also has to encompass the dielectric perfectly. If the housing is too loose, the dielectric can move, while a too tight housing will exert stress on the material, changing its properties. Both requirements cannot be met simultaneously for a housing with a fixed length. Therefore, the cavities reported here are closed using a screw cap, which ensures a good electric contact while the cap is tightened. Shown in Fig. 2 are some cavity designs. From left to right are (1) the old design, (2) a screw cap housing which can either be used as a single or dual mode cavity, and (3) a design optimized for power consumption.

TABLE I. Comparison of vacuum cavities and dielectric cavities at 3 GHz. Shown here are both the theoretical values of a pillbox cavity, compared with measurements performed on optimized shapes.

	Vacuum cavity		Dielectric cavity	
	Pillbox[a]	Optimized	Pillbox[a]	Optimized
Radius (mm)	60.98	66.20	10.16	36.80
P/B_0^2 (10^6 W T^{-2})	43.7	18.0 ± 0.1	3.85	1.67 ± 0.04

[a]Theoretical values from Eqs. (2)–(7) using $\sigma = 5.8 \times 10^7$ S/m, $\varepsilon_r = 36$, and $\tan\delta = 1 \times 10^{-4}$.

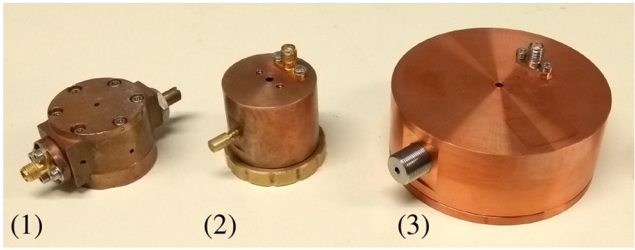

FIG. 2. From left to right: (1) the previous cavity design, (2) the current design using a screw cap, and (3) a low-loss cavity. All are filled with a dielectric material and allow for operation at 3 GHz.

In this paper, the screw cap cavity design is discussed. It is shown that control over the stress applied to the dielectric is crucial for a reproducible design. All important parameters of the dielectric cavity are characterized, and a cavity is demonstrated for implementation in a 3 GHz UEM. Furthermore, two more advanced cavities are presented. The first is a dual mode cavity, which can be used to create pulses at either 3 GHz or 75 MHz, and the second is a cavity optimized for low power consumption, allowing for larger field strengths to be generated.

II. THEORY

A. Uniformly filled cavity

For a cylindrical cavity, the fields of an electromagnetic standing wave can be described in terms of the Bessel functions J_n and Y_n. For a uniformly filled cavity, the field components of the TM_{110} mode in cylindrical coordinates can be written as

$$\begin{aligned} E_z &= \frac{2\omega B_0}{k} J_1(kr)\cos(\theta)\cos(\omega t), \\ B_r &= \frac{2B_0}{kr} J_1(kr)\sin(\theta)\sin(\omega t), \\ B_\theta &= \frac{2B_0}{k} J_1'(kr)\cos(\theta)\sin(\omega t), \end{aligned} \tag{1}$$

with B_0 the maximum magnetic field strength, ω the angular frequency, and $k = \sqrt{\mu\varepsilon}\omega$ the wavenumber, with μ and ε the magnetic permeability and electric permittivity of the medium inside the cavity. The wavenumber and angular frequency of the mode are then given by the requirement that the electric field parallel to the metallic boundary is zero, i.e., $k = j_{1,1}/R$, with R the radius of the cavity and $j_{m,n}$ the nth root of the mth Bessel function. Figure 3 shows the field distribution of the TM_{110} mode.

An important figure of merit for a resonant cavity is the quality factor Q, which relates the time-averaged energy W stored in the cavity to the power loss P_{loss}. The quality factor is defined as

$$Q = \frac{\omega W}{P_{\text{loss}}}. \tag{2}$$

As the electric energy W_e and magnetic energy W_m stored at resonance are equal, the total energy stored in the volume V of the TM_{110} mode is given by[33]

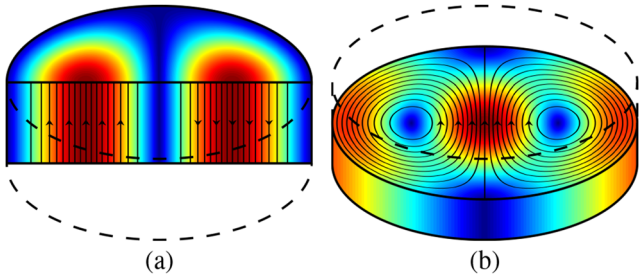

FIG. 3. (a) Longitudinal electric and (b) transverse magnetic field distribution of the TM_{110} mode.

$$W = 2W_e = \frac{1}{2}\int_V \varepsilon_0\varepsilon_r |\mathbf{E}|^2 \, \mathrm{d}^3x \tag{3}$$

$$= \frac{B_0^2\omega^2}{k^2}\varepsilon_0\varepsilon_r \pi R^2 L J_0^2(j_{1,1}). \tag{4}$$

Power losses arise from currents induced in the metallic walls by the magnetic field in the cavity. These losses are given by

$$P_{\text{surface}} = \frac{1}{2}\int_S \frac{|\mathbf{n}\times\mathbf{B}|^2}{\mu^2\sigma\delta_{\text{skin}}} \, \mathrm{d}^2x, \tag{5}$$

$$= \frac{2\pi B_0^2 R}{\mu^2\sigma\delta_{\text{skin}}}(R+L)J_0^2(j_{1,1}), \tag{6}$$

where σ is the conductivity of the wall and $\delta_{\text{skin}} = \sqrt{\frac{2}{\mu\omega\sigma}}$ is the skin depth.

By filling the cavity with a dielectric material, the total surface area decreases, resulting in a reduced power loss in the metallic walls. However, some additional power will also be dissipated by the dielectric material itself. Writing the permittivity as a complex number, power losses arise from a finite imaginary component.[34] Using the so-called loss tangent $\tan\delta = \mathrm{Re}(\varepsilon_r)/\mathrm{Im}(\varepsilon_r)$, the resulting dielectric loss is given by

$$P_{\text{volume}} = \frac{1}{2}\omega\varepsilon_0\varepsilon_r \tan\delta \int_V |\mathbf{E}|^2 \, \mathrm{d}^3x, \tag{7}$$

$$= \frac{\omega^3 B_0^2}{k^2}\varepsilon_0\varepsilon_r \tan\delta \, \pi R^2 L J_0^2(j_{1,1}). \tag{8}$$

In order to reduce the total power consumption, the dielectric material therefore needs to have both a sufficiently large ε_r and a sufficiently low $\tan\delta$, such that the decrease in surface losses is greater than the increase in volume losses.

B. Partially filled cavity

In practice, the cavity cannot be filled uniformly as electrons have to pass through the center. Furthermore, leaving space around the dielectric material allows for the insertion of an antenna and a tuning stub. In this section, we will calculate the field distribution and power consumption using the geometry as shown in Fig. 4(b), where a dielectric of radius R_d with a central hole of radius R_h is placed at the center of a cavity with outer radius R_c.

For a nonuniform cylindrical cavity with a circularly symmetric cross-section, the field solutions can still be described in terms of the

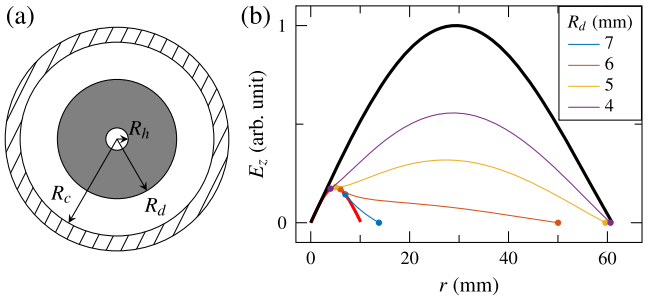

FIG. 4. (a) Geometry of the partially filled cavity. A dielectric with radius R_d is placed in a metallic cavity of radius R_c. In the center, there is a hole with radius R_h. (b) Electric field as a function of radius for several partially filled cavities, with the circles at the start and end denoting R_d and R_c. Also shown is the field of a vacuum cavity (black) and a dielectric cavity (red). The magnetic field strength at $r = 0$ and the frequency are fixed for each curve.

Bessel functions of the first and second kind J_ν and Y_ν. For the TM_{110} mode, the longitudinal electric fields in the three different regions are now given by

$$E_z(r,\theta) = 2cB_0\cos(\theta) \times \begin{cases} J_1(k_0 r) & \text{if } r \le R_h, \\ \left[AJ_1(\sqrt{\varepsilon_r}k_0 r) + BY_1(\sqrt{\varepsilon_r}k_0 r)\right] & \text{if } R_h < r \le R_d, \\ \left[CJ_1(k_0 r) + DY_1(k_0 r)\right] & \text{if } R_d < r \le R_c, \end{cases} \quad (9)$$

where k_0 is the wavenumber in a vacuum. This equation is subject to the boundary condition that the electric field parallel to the surface is continuous, i.e., $E_z(R_h)$ and $E_z(R_d)$ are continuous. Furthermore, due to the absence of surface currents on the dielectric, the magnetic field is also continuous, implying that $E_z'(R_h)$ and $E_z'(R_d)$ are continuous. These four requirements determine the constants A, B, C, and D. Although analytical expressions exist for these constants,[35] they will not be given here. The wavenumber k_0 is again determined by the requirement that $E_z(R_c) = 0$ and has to be found numerically. Figure 4(b) shows the fields of Eq. (9) for several values of R_d, together with the solutions of the vacuum cavity, and the dielectric cavity with a central hole $R_h = 1.5$ mm. Here, both B_0 and k_0 are fixed, in which case the constants A and B are also fixed, resulting in the same field distribution within the dielectric. Colored circles in the graph show the positions of R_d and R_c.

Varying R_d and R_c in such a way that the resonant frequency is kept constant allows for an interesting solution to be found, in which the electric field amplitude reaches its maximum inside the dielectric material and slowly decays toward the wall, resulting in small magnetic fields outside the dielectric material. This can be seen from Fig. 5 for the values of R_d of 7 and 6. Because the magnetic field scales with the gradient of the electric field, these solutions will have smaller magnetic fields near the outside wall of the cavity, reducing the surface losses. An optimum therefore exists, where the outer radius of the cavity is small enough to suppress the standing wave outside the dielectric, but large enough to separate the walls from the large magnetic fields inside the dielectric.

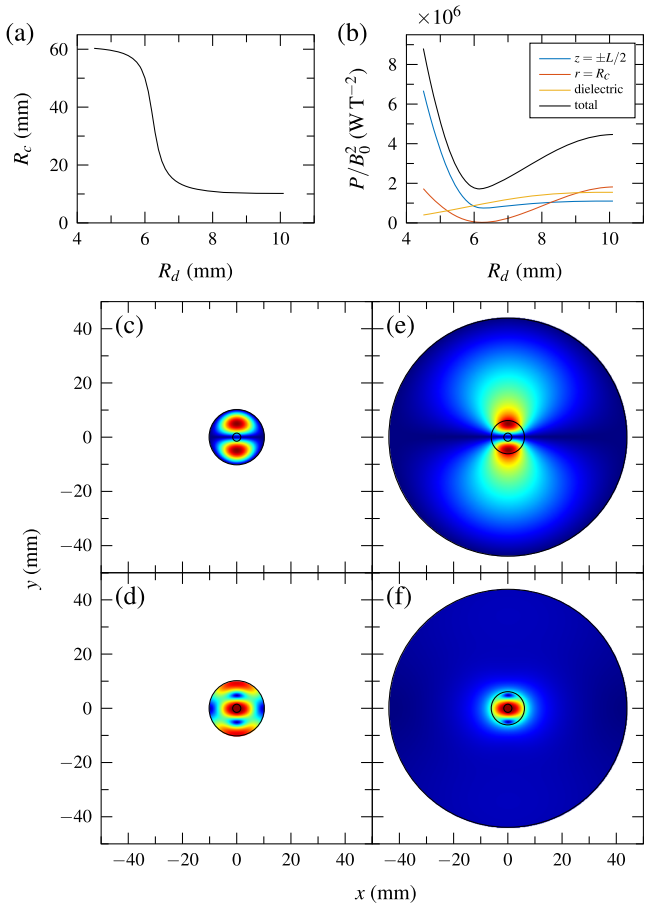

FIG. 5. (a) Cavity size and (b) power consumption per unit of magnetic field squared as a function of dielectric radius R_d when keeping the resonant frequency fixed at 3 GHz. The power consumption is split into three contributions, namely, surface losses at the top and bottom of the cavity ($z = \pm L/2$), surface losses at the side ($r = R_c$), and volume losses due to the dielectric. (c) Electric and (d) magnetic field distribution of a dielectric cavity, compared to (e) and (f) those of an optimized cavity.

The effect of varying R_d on both R_c and on the power consumption is shown in Figs. 5(a) and 5(b). The power consumption is split into three contributions, showing that the decrease is mostly due to the reduced losses at $r = R_c$. As the outer cavity radius R_c approaches that of a vacuum cavity, losses go up again due to the emergence of strong magnetic fields outside the dielectric. Figures 5(c)–5(f) show the electric and magnetic field distributions for both a completely filled dielectric cavity and a partially filled cavity with an optimized geometry. In all these figures, the dielectric material has been assumed to have $\varepsilon_r = 36$ and $\tan\delta = 1 \times 10^{-4}$, and the cavity length has been chosen to be $L = 16.67$ mm. For these numbers, optimizing the filling ratio allows for a further reduction in power consumption by a factor of 2.6. As a comparison, the optimized cavity requires an input power of 15.5 W to generate a field strength of 3 mT, whereas a vacuum pillbox equivalent would require 393 W.

C. Electron beam dynamics

When an electron beam moves through the center of the cavity, the electrons will experience a transverse Lorentz force. Assuming that the size of the electron beam is much smaller than that of the cavity, all electrons feel approximately the on-axis field, which is given by

$$\vec{B} = B_0 \sin(\omega t + \phi)\hat{y}, \tag{10}$$

where a phase shift ϕ has been added between the arrival time of the electron and the fields in the cavity. This results in a Lorentz force acting on the electrons given by

$$\vec{F}_L = -q_e v_z B_0 \sin(\omega t + \phi)\hat{x}, \tag{11}$$

with q_e the electron charge and v_z the longitudinal velocity. Assuming that the cavity has a top-hat field profile running from $-L/2 < z < L/2$ and assuming that the change in the longitudinal velocity inside the cavity is negligible, the total force exerted on the electrons causes a transverse change in the velocity given by

$$v_x = -\frac{2q_e v_z B_0}{\gamma m_e \omega} \sin(\phi) \sin\left(\frac{\omega L}{2v_z}\right), \tag{12}$$

with γ the Lorentz factor of the electrons and m_e the electron mass. A maximum deflection is achieved for a cavity length $L = \pi v_z/\omega$, i.e., when the electron transit time is half the oscillation period of the cavity. Placing a slit of width s at a distance d, the resulting pulse length can then be approximated by

$$\tau = \frac{\gamma m_e s}{2|q_e| B_0 d \sin(\omega L/2v_z)}. \tag{13}$$

Given a slit of $s = 10$ μm placed at a distance of $d = 10$ cm and electrons with $\gamma \approx 1$, a field strength of $B_0 = 3$ mT is then required for pulses of $\tau \approx 100$ fs.

III. CAVITY DESIGN

The cavities presented here are filled with a $ZrTiO_4$ ceramic doped with <20% $SnTiO_4$ produced by the company T-Ceram.[36] The relative permittivity is quoted as $\varepsilon_r = 36.5$–38 in the frequency range of 0.9–18 GHz, with a loss tangent of $\tan\delta = 2 \times 10^{-4}$ measured at 10 GHz.

Currently, the dielectric cavities are used both in a 200 keV UEM and a 30 keV electron beam setup. The cavity length is therefore chosen to be $L = 16.67$ mm, close to the optimal length for 30 keV electrons. Although a longer cavity length would increase the deflection of 200 keV electrons, this is not necessarily beneficial for the quality of the electron pulses.[22] Therefore, the reduction to ~68% of the maximum deflection for 200 keV electrons is considered acceptable.

Figure 6(a) shows a schematic cut-through of a cavity. Each cavity consists of a cylindrical dielectric placed inside a larger metal housing which is open from the bottom. Ample room is left around the dielectric to also insert an antenna and a tuning stub. As will be demonstrated in Sec. IV, the ability to control the stress applied to the dielectric is of paramount importance. Therefore, the cavity is closed using a cap with a screwing thread in the side which is tightened using a torque wrench, allowing for the stress to be applied controllably while the cap remains electrically connected.

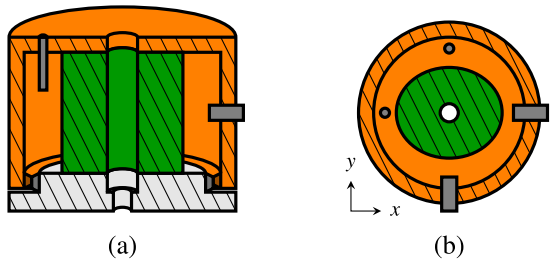

FIG. 6. (a) Cross section of the screw cap design, with the dielectric in dark green, copper housing in orange, screw cap in light gray, and a linear antenna and a tuning stub in dark gray. (b) Top view of the dual mode cavity, which is filled with an elliptical dielectric. Shown in dark gray are the antenna and tuning stub along both the short and long axes of the dielectric.

Inside the UEM, the cavity is powered by using a Mini-Circuits ZHL-16W-43-S+ amplifier, delivering up to 16 W of power. Because the cavity is inserted in a vacuum of the microscope, water cooling is needed to prevent excessive heating of the cavity and the microscope. Furthermore, the small bandwidth of the cavity results in a large phase shift when the resonance drifts away from the drive frequency due to temperature fluctuations. For a typical cavity, a 100 fs temporal stability requires ~mK temperature stability.[37] This is the second reason for using the water cooler, which is designed for a temperature stability of <1 mK.

The cooling water can run either through the housing or through a heat sink connected to the screw cap. Power is coupled into the cavity using a linear antenna, and the frequency can be tuned several megahertz using a metal tuning stub.

A hole at the center of 3 mm is used for the electrons to pass through. The housing, dielectric, and cap are centered during the assembly through these holes with a small rod. Furthermore, it is important to prevent electrons from hitting the dielectric to avoid charging. Therefore, the hole in the cap is narrowed to 2 mm on the outside. On the side of the dielectric, the hole is 3 mm to avoid an asymmetry in the fringe fields at the entrance and exit.

Figure 6(b) shows a top view of a dual mode cavity. Instead of a circular cylindrical dielectric, an elliptical cylinder is used to break the degeneracy of the differently oriented modes. Along the short and long axes, an antenna and a tuning stub are placed, giving nearly independent control over each mode. In case of a single mode cavity, only one antenna and a tuning stub are inserted.

For the cavities, a linear antenna is used. It can be shown that the field excited in the cavity by a linear antenna is given by[38]

$$e_0 = -j\omega\mu_0 \frac{\int_V \vec{J}(\vec{r}) \cdot \vec{E}_n(\vec{r})\, \mathrm{d}v}{k_0^2 - k^2\left(1 + \frac{1-j}{Q_0}\right)}, \tag{14}$$

where e_0 is the amplitude of the solenoidal electric mode $\mathbf{E}_n$ normalized by volume, which has a wavenumber k_0 and a quality factor Q_0, and $\mathbf{J}$ is the current distribution of the antenna. Furthermore, ω and k are the angular frequency and wavenumber of the excitation signal. Although solving this equation relies on exact knowledge of the

current distribution in the cavity and therefore the fields around the antenna, which are not known analytically, it shows that modes that have a high electric field at the antenna location are mostly excited.

Although the field strength per unit of current on the antenna is maximized by placing the antenna at the electric field maximum, this is not the ideal situation, as the cavity will likely become overcoupled, reducing the power transfer. The criterion for an antenna operating at high input power is therefore that its impedance is matched. Matching can be expressed in terms of the coupling factor g, which is given by

$$g = \frac{1 - |\Gamma_v|}{1 + |\Gamma_v|}, \tag{15}$$

where Γ_v is the voltage reflection coefficient. In practice, impedance matching is done by taking an antenna which is overcoupled and then decreasing the length incrementally until the reflected power drops below a desired value. Once matched, the reflected power at resonance typically remains below a few percent during operation. Although in this design the antennas are placed outside the dielectric material where the electric field is low, overcoupling is relatively easy to achieve with a 50 Ω RF setup.

IV. CHARACTERIZATION

A. Screw cap design

The most important reason to use the screw cap design is to improve reproducibility in both fabrication and assembly. In order to test this, two cavities were fabricated and five dielectrics accurately machined to a radius of $R_d = 7.5$ mm were placed inside both cavities. Assembly of each combination was repeated four times. Figure 7(a) shows the resulting average resonant frequency and the standard deviation for each of the dielectrics, with the two cavity housings shown in different colors. The right axis shows the corresponding relative permittivity of the dielectrics estimated using simulations. All simulations are performed with CST Microwave Studio software[39] (MWS), which solves Maxwell's equations using finite element methods. Due to the high quality factor, all simulations are performed in the frequency domain, solving for the steady state behavior.

The differences in the cavity housings result in a systematic frequency difference of 2.4 ± 0.9 MHz, well within the tuning range. Unfortunately, different pieces of dielectric deviate more. It is currently unknown whether this difference arises from machining inaccuracies, damages, or chips in the material, or differences in the relative permittivity of the dielectric. Figure 7(b) shows a histogram of the deviation from the average resonant frequency for each configuration. This shows that assembling the cavity can be done reproducibly within a few megahertz.

To test the influence of stress on the dielectric, the resonant frequency of one of these cavities was measured as a function of the closing torque applied to the cap. This is shown in Fig. 8(a). This shows that with the application of stress on the dielectric, the frequency drops drastically. Control over the stress applied on the dielectric is therefore critical for a reproducible design.

Figure 8(b) shows the change in the resonant frequency as a function of the temperature of the cavity, performed at two different closing torques. For a copper vacuum cavity, the change is expected to be −50 kHz/K due to thermal expansion of the copper, whereas a change of 373 ± 9 kHz/K and 250 ± 3 kHz/K is found for a small and large stress, respectively. Although the permittivity of the material changes with different temperatures, this is typically only a few ppm and is therefore not expected to have a large influence. The change is therefore attributed to the different thermal expansions of the dielectric and the housing, causing a change in stress on the material. Although this larger change in the resonant frequency increases the tunability of the cavity through temperature, it also means that the requirements on thermal stability increase.

Next, a cavity was designed to be implemented in a TEM. The two requirements on this cavity are that its resonant frequency must lie at 2.9985 GHz to allow for synchronization to a laser system and that large powers can be coupled into the cavity. Shown in Figs. 9(a) and 9(b) are the resonant frequency and coupling factor of the cavity for varying stub and antenna lengths, respectively. With the stub, the resonant frequency can be increased by up to 10.38 ± 0.01 MHz. With the antenna, the impedance of the cavity can be accurately matched to minimize power reflection.

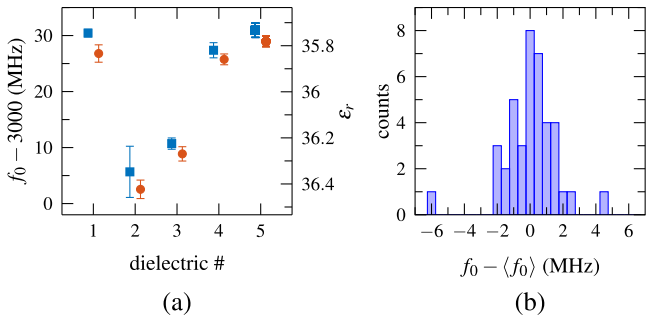

FIG. 7. (a) Resonant frequency for five different pieces of dielectric (in random order), each placed in one of two cavities. Each combination was assembled four times. The right y-axis shows the corresponding relative permittivity as estimated using simulations. (b) Histogram of the deviations of all measured resonant frequencies from the average of each configuration.

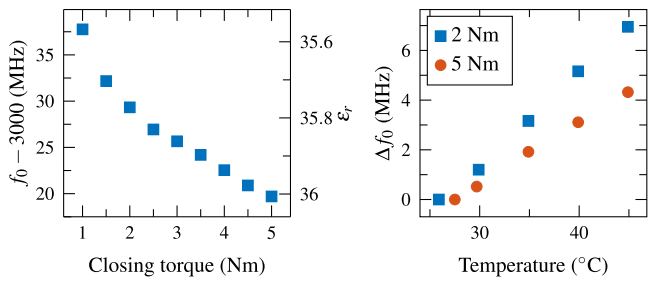

FIG. 8. (a) Resonant frequency as a function of the closing torque applied to the screw cap. (b) Resonant frequency as a function of temperature for a cavity closed with two different torques.

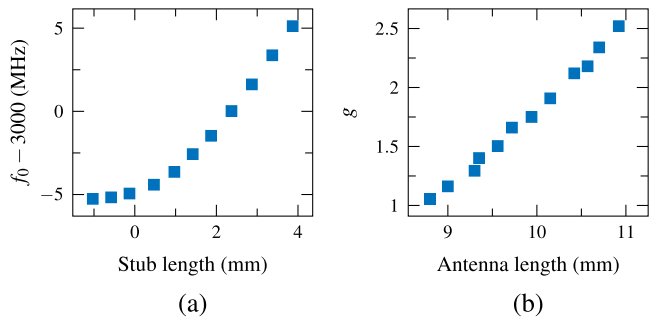

FIG. 9. (a) Resonant frequency as a function of stub depth. (b) Coupling factor as a function of the antenna length.

Shown in Fig. 10 is the power reflection of the cavity tuned for insertion in an UEM, showing that the cavity can be tuned to accept power at the desired frequency. The absorbed power P_{abs} as a function of frequency f can be fitted with

$$\frac{P_{abs}}{P_{inc}} = 1 - |\Gamma_v|^2 = \frac{4g}{(1+g)^2} \frac{1}{\frac{4Q^2}{(1+g)^2 f_0^2}(f-f_0)^2 + 1}, \quad (16)$$

with P_{inc} the incoming power and f_0 the resonant frequency. From the fit, the quality factor is determined to be $Q = (2.82 \pm 0.04) \times 10^3$. Comparing this with simulations, the loss tangent of the material is then expected to be $\tan\delta = (2.38 \pm 0.05) \times 10^{-4}$. However, the actual loss tangent is expected to be slightly lower, as the measured quality factor tends to be lower than simulations,[32] likely due to small imperfections.

The performance of this cavity inside a TEM has been reported in Ref. 17. The same design was reproduced multiple times, allowing for the use of two TM_{110} mode cavities synchronized to a TM_{010} mode compression cavity, as reported in Ref. 17.

B. Dual mode cavity

Next, a dual mode cavity was designed. For a rotationally symmetric cavity, there is no preferential direction for the modes. Due to the presence of the antenna and stub this degeneracy is broken, fixing the mode orientation. Typically, a small transverse component remains, likely due to imperfections, giving rise to a slightly elliptical streak.[19] For the dual mode cavity, however, the cavity shape is modified to shift the frequency of one orientation. This is currently done by making the dielectric material elliptical and placing it in a circular housing, as shown in Fig. 6(b). Along the short axis of the dielectric, the frequency is then increased. This is done in such a way that the lower frequency can be synchronized to the 40th harmonic of a 75 MHz laser oscillator and the higher frequency to the 41st harmonic.

To induce the correct frequency shift in the perpendicular mode, a dielectric was fabricated with a short semiaxis of 7.030 ± 0.005 mm and a long semiaxis of 7.575 ± 0.005 mm. With these dimensions, the same housing can be used as for the single-mode dielectrics with a radius of 7.5 mm.

The 40th harmonic of the cavity can be excited using a microwave-to-laser synchronization system.[23–25] The 41st harmonic is excited by mixing the laser frequency with the synchronized 40th harmonic, which outputs both the sum and difference frequencies. Although performance is not expected to drop due to the presence of the difference frequency, it has a small but noticeable effect on the Lissajous pattern. Therefore, an image rejection mixer is used in our setup to suppress the difference frequency.

Figure 11 shows the power reflection as a function of frequency for the two different antennas of a dual mode cavity. As can be seen, each antenna can strongly excite one of the two perpendicular modes and couples a negligible amount of power into the other mode. Also present in this frequency range is a mode which is assumed to be a TE_{010} mode. However, it is located several tens of megahertz away from the TM_{110} modes that its presence is not noticeable during operation.

In order to test the dual mode cavity, it was inserted in a beamline, in which an electron beam is generated using the column of a Philips XL-30 SEM. A special vacuum flange was made with feedthroughs for the cooling water and the two RF signals. Using the SEM column, the electron beam is then focused through the cavity onto a MediPix detector.

Shown in Fig. 12 is the electron beam on the detector after passing through the dual mode cavity with power fed into both modes

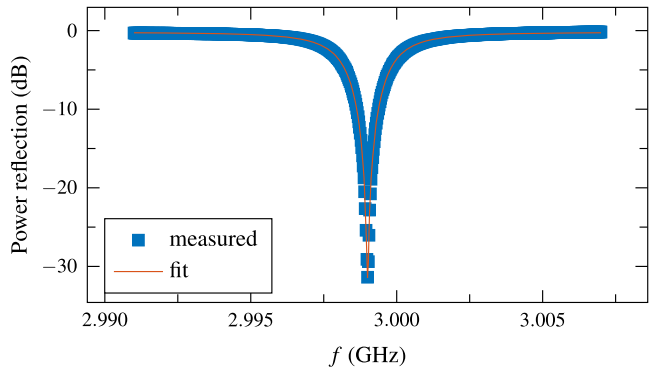

FIG. 10. Power reflection as a function of frequency, showing that good coupling can be obtained at the desired frequency. From the fit, the quality factor of the cavity has been determined to be $(2.82 \pm 0.04) \times 10^3$.

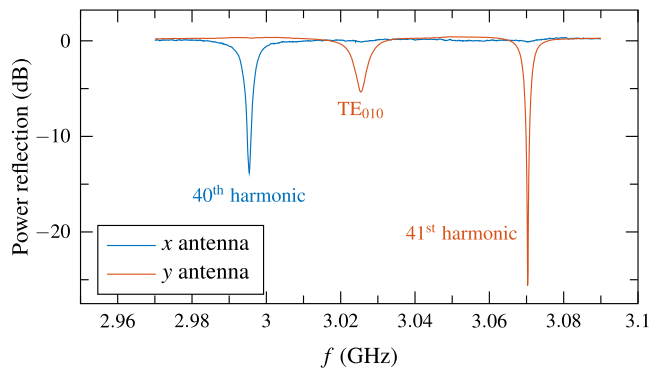

FIG. 11. Reflection parameter of a dual mode cavity as seen through the two antennas. Apart from the two perpendicular TM_{110} modes, a different mode is also visible, assumed to be a TE_{010} mode.

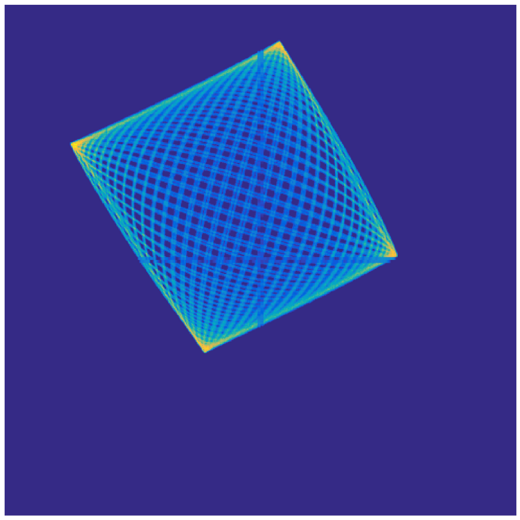

FIG. 12. Electron beam deflected onto a detector following the Lissajous pattern.

synchronized to the laser system. This shows that both can indeed be accurately mode-locked to result in a deflection following a Lissajous pattern. In Ref. 30, both the synchronization system and the performance of a dual mode cavity as a beam blanker in a TEM are presented. Furthermore, the dual mode cavity can be used as a streak camera with a huge field of view, allowing for the full range of 13 ns to be imaged with 100 fs resolution.

C. Low loss cavity

Finally, an optimized cavity design was manufactured and tested in the same beamline as the dual mode cavity. For this, a dielectric with a radius of $R_d = 6.25$ mm was made and placed in a cavity of radius $R_c = 36.8$ mm. The magnetic field strength was then measured by deflecting the 30 keV electron beam onto a detector over a distance of $d = 271 \pm 5$ mm. With the cavity length optimized for 30 keV electrons, the field strength can then be calculated from the length of the streak L_{streak} on the detector using

$$B_0 = \frac{\gamma m_e \omega}{4|q_e|d} L_{\text{streak}}. \tag{17}$$

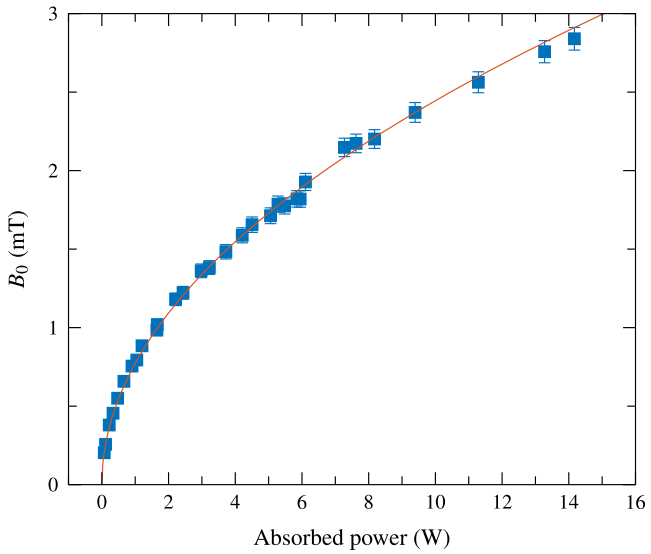

FIG. 13. Magnetic field strength as a function of input power of a cavity optimized for low power loss.

TABLE II. Simulated and measured properties of the low-loss cavity. For the simulations, $\varepsilon_r = 35.55$ and $\tan\delta = 1 \times 10^{-4}$ are used.

	MWS	Measured
f_0 (GHz)	2.995	2.9998
Q	6.00×10^3	$(5.02 \pm 0.04) \times 10^3$
P/B_0^2 (10^6 W T^{-2})	1.79	1.67 ± 0.04

Shown in Fig. 13 is the magnetic field strength of this cavity as a function of the input power. The solid line shows a fit of the data using $B_0 \propto \sqrt{P}$, from which the power loss is found to be $P/B_0^2 = (1.67 \pm 0.04) \times 10^6$ W T^{-2}. This is considerably lower than the value of $(18.0 \pm 0.1) \times 10^6$ W T^{-2} that can be reached in an optimized vacuum cavity, showing the main advantage of using a dielectric material.

At a total input power of $P = 14.2 \pm 0.2$ W, a magnetic field of $B_0 = 2.84 \pm 0.07$ mT was achieved. Deflecting an electron beam over a 10 μm slit with this cavity would result in a pulse length of $\tau = 106 \pm 3$ fs at 30 keV or $\tau = 204 \pm 5$ fs at 200 keV. Table II summarizes the properties of the optimized cavity compared to the expectations from MWS simulations.

V. CONCLUSIONS

A robust and reproducible design for a dielectric microwave cavity has been presented. Control over the resonant frequency of the cavity is crucial for synchronization to a laser system or other cavities. Furthermore, the robustness of the cavities allows for better characterization of the dielectric material, enabling more advanced cavity designs. Two of these advanced designs were also presented.

The first, called the dual mode cavity, supports two perpendicular modes at different well-defined frequencies. This allows for streaking the electron beam in a Lissajous pattern, extending the range of pulse repetition rates that can be achieved with a cavity. The second design was optimized for low losses. With this design, losses were reduced to $P/B_0^2 = (1.67 \pm 0.04) \times 10^6$ W T^{-2}, and field strengths up to $B_0 = 2.84 \pm 0.07$ mT were demonstrated.

The reproducibility is limited by the dielectric material, which showed by far the largest deviations for currently unknown reasons. However, the tuning range achievable with the combination of a stub, the controlled application of mechanical stress, and the temperature are large enough to correct for these deviations. Alternatively, these deviations can be overcome by first characterizing each dielectric in a test cavity, after which a housing can be custom made.

ACKNOWLEDGMENTS

This work was part of an Industrial Partnership Programme of the Foundation for Fundamental Research on Matter (FOM), which is part of The Netherlands Organisation for Scientific Research (NWO).

REFERENCES

[1]O. Scherzer, Z. Phys. **101**, 593 (1936).
[2]P. W. Hawkes, Philos. Trans. R. Soc., A **367**, 3637 (2009).
[3]L. Oldfield, J. Phys. E: Sci. Instrum. **9**, 455 (1976).
[4]K. Ura and N. Morimura, J. Vac. Sci. Technol. **10**, 948 (1973).
[5]T. Hosokawa, H. Fujioka, and K. Ura, Rev. Sci. Instrum. **49**, 624 (1978).
[6]A. H. Zewail, Annu. Rev. Phys. Chem. **57**, 65 (2006).
[7]D. J. Flannigan and A. H. Zewail, Acc. Chem. Res. **45**, 1828 (2012).
[8]B. Siwick, J. R. Dwyer, R. E. Jordan, and R. J. D. Miller, Science **302**, 1382 (2003).
[9]Y. Morimoto and P. Baum, Nat. Phys. **14**, 252 (2018).
[10]F. Carbone, B. Barwick, O. Kwon, H. S. Park, J. S. Baskin, and A. H. Zewail, Chem. Phys. Lett. **468**, 107 (2008).
[11]R. M. van der Veen, T. J. Penfold, and A. H. Zewail, Struct. Dyn. **2**, 024302 (2015).
[12]G. Berruto, I. Madan, Y. Murooka, G. M. Vanacore, E. Pomarico, J. Rajeswari, R. Lamb, P. Huang, A. J. Kruchkov, Y. Togawa, T. LaGrange, D. McGrouther, H. M. Rønnow, and F. Carbone, Phys. Rev. Lett. **120**, 117201 (2018).
[13]T. van Oudheusden, P. L. E. M. Pasmans, S. B. van der Geer, M. J. de Loos, M. J. van der Wiel, and O. J. Luiten, Phys. Rev. Lett. **105**, 264801 (2010).
[14]P. Musumeci, J. T. Moody, C. M. Scoby, M. S. Gutierrez, M. Westfall, and R. K. Li, J. Appl. Phys. **108**, 114513 (2010).
[15]J. Maxson, D. Cesar, G. Calmasini, A. Ody, P. Musumeci, and D. Alesini, Phys. Rev. Lett. **118**, 154802 (2017).
[16]W. Verhoeven, J. F. M. van Rens, M. A. W. van Ninhuijs, W. F. Toonen, E. R. Kieft, P. H. A. Mutsaers, and O. J. Luiten, Struct. Dyn. **3**, 054303 (2016).
[17]W. Verhoeven, J. F. M. van Rens, E. R. Kieft, P. H. A. Mutsaers, and O. J. Luiten, Ultramicroscopy **188**, 85 (2018).
[18]A. Feist, N. Bach, N. R. da Silva, T. Danz, M. Möller, K. E. Prieve, T. Domröse, J. G. Gatzmann, S. Rost, J. Schauss, S. Strauch, R. Bormann, M. Sivis, S. Schäfer, and C. Ropers, Ultramicroscopy **176**, 63 (2017).
[19]A. C. Lassise, "Miniaturized RF technology for femtosecond electron microscopy," Ph.D. thesis, Eindhoven University of Technology, 2012.
[20]J. Qui, G. Ha, C. Jing, S. V. Baryshev, B. W. Reed, J. W. Lau, and Y. Zhu, Ultramicroscopy **161**, 130 (2015).
[21]I. G. C. Weppelman, R. J. Moerland, J. P. Hoogenboom, and P. Kruit, Ultramicroscopy **184**, 8 (2018).
[22]J. F. M. van Rens, W. Verhoeven, J. G. H. Franssen, A. C. Lassise, X. F. D. Stragier, E. R. Kieft, P. H. A. Mutsaers, and O. J. Luiten, Ultramicroscopy **184**, 77 (2018).
[23]G. J. H. Brussaard, A. C. Lassise, P. L. E. M. Pasmans, P. H. A. Mutsaers, M. J. van der Wiel, and O. J. Luiten, Appl. Phys. Lett. **103**, 141105 (2013).
[24]M. Walbran, A. Gliserin, K. Jung, J. Kim, and P. Baum, Phys. Rev. Appl. **4**, 044013 (2015).
[25]M. R. Otto, L. P. René de Cotret, M. J. Stern, and B. J. Siwick, Struct. Dyn. **4**, 051101 (2017).
[26]C. Kisielowski, P. Specht, B. Freitag, E. R. Kieft, W. Verhoeven, J. F. M. van Rens, P. H. A. Mutsaers, O. J. Luiten, S. Rozeveld, J. Kang, A. J. McKenna, P. Nickias, and D. F. Yancey, Adv. Funct. Mater. **29**, 1807818 (2019).
[27]E. van den Bussche and D. Flannigan, "Reducing radiation damage in soft matter with femtosecond timed single-electron packets," ChemRxiv:8079755 (2019).
[28]M. S. Grinolds, V. A. Lobastov, J. Weissenrieder, and A. H. Zewail, Proc. Natl. Acad. Sci. U. S. A. **103**, 18427 (2006).
[29]D. R. Cremons, D. A. Plemmons, and D. J. Flannigan, Nat. Commun. **7**, 11230 (2016).
[30]J. F. M. van Rens, W. Verhoeven, E. R. Kieft, P. H. A. Mutsaers, and O. J. Luiten, Appl. Phys. Lett. **113**, 163104 (2018).
[31]A. C. Lassise, P. H. A. Mutsaers, and O. J. Luiten, Rev. Sci. Instrum. **83**, 043705 (2012).
[32]T. van Oudheusden, "Electron source for sub-relativistic single-shot femtosecond diffraction," Ph.D. thesis, Eindhoven University of Technology, 2010.
[33]D. M. Pozar, *Microwave Engineering*, 4th ed. (Wiley, 2012).
[34]D. J. Griffiths, *Introduction to Electrodynamics*, 3rd ed. (Pearson, 2008).
[35]R. G. Carter, IEEE Trans. Microwave Theory Tech. **49**, 918 (2001).
[36]See http://www.t-ceram.com/dielectric-resonators.htm for company information (last accessed October 2018).
[37]P. L. E. M. Pasmans, "Ultrafast electron diffraction: An investigation of fundamental limits," Ph.D. thesis, Eindhoven University of Technology, 2014.
[38]R. E. Collin, *Foundations for Microwave Engineering*, 2nd ed. (Wiley, 2001).
[39]See http://www.cst.com/products/cstmws for information on the software (last accessed October 2018).